Design of Multiband Antenna using Fringing Effects of Metamaterials

Dang Nhu Dinh[1,2], Hoang Phuong Chi[1], Dao Ngoc Chien[3]*
[1]*Hanoi University of Science and Technology, No. 1, Dai Co Viet, Hanoi, Viet Nam*
[2]*The University of Fire Fighting and Prevention, No. 243, Khuat Duy Tien, Hanoi, Viet Nam*
[3]*Ministry of Science and Technology, No. 113, Tran Duy Hung, Hanoi, Viet Nam*
Received: June 06, 2016; accepted: June 9, 2017

Abstract

A design of multiband microstrip antenna based on fringing effects of metamaterials is proposed in this paper. The proposed antenna is printed on FR4 substrate with a dielectric constant of 4.4 and a thickness of 1.6 mm. The antenna is constructed by two spiral branches and each branch are composed by many strip segments. The resonant frequency bands of proposed antenna can be calculated and controlled by using fringing effects of metamaterials that depends on the value of the gap between the segments of each spiral branch. Besides, mutual induction is used to suppress the harmonics between the designed frequencies in order to create a multiband resonance. The proposed antenna is optimized to operate at the frequency bands of 4G (1.8 GHz), WLAN (2.4 GHz) and WiMAX (3.5 GHz). The measured S11 of fabricated antenna shows that the antenna can resonate at three -10 dB bandwidths of (1.70 – 1.96) GHz, (2.34 – 2.57) GHz and (3.43 – 3.78) GHz.

Keywords: Fringing effects, Metamaterials, Multiband antenna

1. Introduction

Regarding the trend of multi-service integration, besides the requirements of compact size and easy fabrication, the devices of the wireless communication systems should be designed to operate in multiple frequency bands. Therefore, the design methodology of multi-band microwave components is always a hot topic of microwave community. In most of proposed designs, microstrip technology is often implemented to design the microwave components, such as antenna, band-pass filter or power divider thanks to its advantages of compactness design and easy fabrication.

In literature, the multi-band microwave components are often based on the traditional methodologies, which has been proposed previously. In case of multiband antennas, many design methodologies have been proposed and applied effectively. In general, there are some basic methods such as creating the slots on radiation surface or ground plane of the substrate [3], using multiple parasitic elements [4, 5], or using the frequency band rejection in broadband structure to create multi-band resonance, in this case, slots are typically used to reject unwanted frequency bands [6, 7]. On the other hand, fractal geometry is one of the methods has been used in multi-band antenna design [8-10].

This paper proposed a new design methodology of multiband antenna based on fringing effects of metamaterials. This method will create an extended area of original excitation area to cover an any region, located near by the excitation one, and make it resonate. In addition, the mutual induction is used to suppress the harmonics to create the multiband resonance. This design methodology does not use slotted structure of parasitic elements as previous studies.

2. Multiband antenna design

2.1. Fringing Effects in Multiband Antenna Design

As simplified way, the current distribution at the outer edge of the surface in the dielectric shown in Fig. 1, making the physical length of the conductor increases a range of Δ .

$$L' = L + \Delta \quad (1)$$

where L is the real length of the conductor, Δ is the length increment caused by fringing effect and L' is the real electrical length of the conductor.

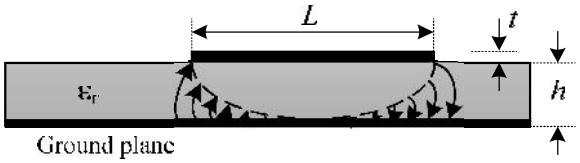

Fig. 1. Fringing effects of metamaterials.

The length increment will alter the limited area of the wave modes in the waveguide. We can calculate this increment by following formula:

*Corresponding author: Tel.: (84) 438692242
Email: chi.hoangphuong@hust.edu.vn

$$\Delta = 0{,}412 \times h \frac{(\varepsilon_e + 0.3)\left(\frac{W}{h} + 0.264\right)}{(\varepsilon_e - 0.258)\left(\frac{W}{h} + 0.8\right)} \quad (2)$$

where ε_r is the effective dielectric constant, and h is the thickness of the substrate. Each different frequency and positive area width W gives us the different length increment.

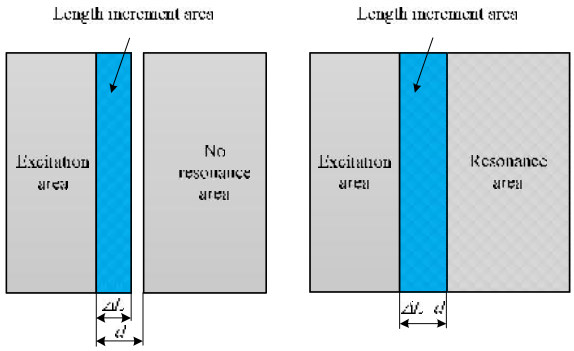

(a) (b)

Fig. 2. (a) No resonance area, and (b) Resonance area.

Fig. 2 represents the relations of fringing effects and the resonant ability of any area, in which Δ is the increment length shown in Eq. (3), and d is the distance between excitation area and any area. As observed in Fig. 2(a), when the length increment of the excitation region is smaller than the distance between the two regions ($\Delta < d$), the fringing effects have not occurred. This means that the region located near the excitation region cannot resonate. Conversely, when $\Delta \geq d$ the fringing effects will occur. In this case, the length increment area of the excitation area has been exposed or covered the any area and make this region resonant as described in Fig. 2(b).

Thus, the fringing effects will occur under the following condition:

$$\Delta \geq d \quad (3)$$

However, depending on the coverage of extended area to the any area is small or big that the influence of fringing effects will vary differently. Thus, by creating different extended area, we can create the resonance at different frequencies. This is the basic theory of the proposed solutions for analysis and design the multiband antenna in this paper.

In the multiband antenna design, basic principle of the solutions is to create different resonant modes on the proposed model. General model in Fig. 3 is used to analyze and calculate the fringing effects of the proposed tri-band antenna.

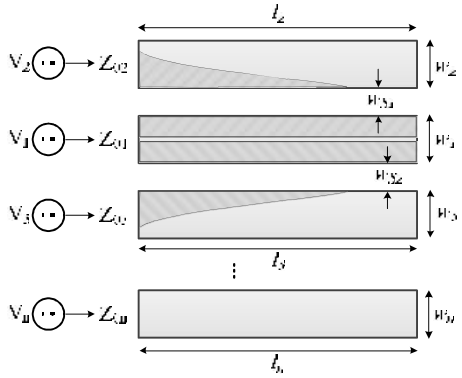

Fig. 3. General model of antenna based on fringing effects.

Assuming V_1 is antenna input source, the radiation efficiency of antenna is μ as in ideal conditions, if we ignore the thermal losses on the antenna, then we have:

$$V_1 = V_0 . e^{j\theta_1} . \cos(\omega_1 t) \quad (4)$$

Assuming λ_i is the resonant wavelength of mode i at the frequency f_i

$$V_n = V_0 . (1 - \Gamma_0) . (1 - \Gamma_0) . (-\Gamma_{0n}) . e^{j\theta_1} . \prod_{j-1}^{n} e^{j2\pi \frac{l_j}{\lambda_i}} . \cos(\omega_i t) \quad (4a)$$

Considering in mode i that are affected by mode (i + 1) and (i - 1) caused by fringing effects as described in Fig. 4. Call δ_i is transmission loss in metamaterials,

$$\delta_i \approx \left(\frac{4\pi}{\lambda_i}\right)^n \quad (5)$$

with d is the spread distance

The input power of mode i is determined as follows,

$$P_{in\,(i)} = \frac{V_i^2}{Z_0} = \frac{V_0^2 . e^{j2\theta_1} \left[\prod_{j-1}^{n} (1 - \Gamma_{0j}) . e^{j2\pi \frac{l_j}{\lambda_i}} . \cos(\omega_i t)\right]^2}{\sum_{j-1}^{n} Z_{0j}} \quad (6)$$

Then, we can calculate the power spreading in the dielectric as

$$P_T = P_{in} (1 - \mu_i) \quad (7)$$

with μ_i is radiation efficiency of the antenna at resonant wavelength λ_i

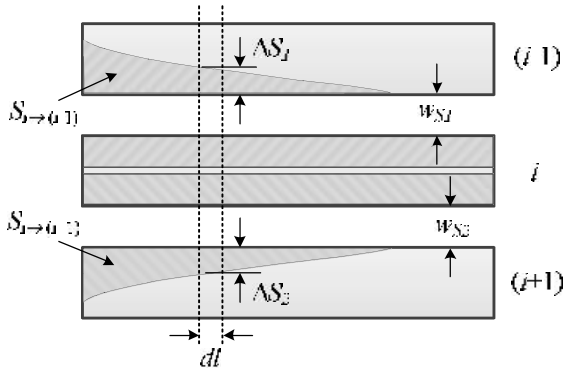

Fig. 4. Describing the fringing effects caused by mode i to mode $(i-1)$ and $(i+1)$

Considering in a very small range of dl with unchanged phase of current, we have

$$d_{m\ (i-1)(i)} = w_{S1} + \Delta_1 \quad (8)$$

The resonance condition is $P_T = 0$ and $\Delta L > w_{S1}$.

where $d_{m\ (i-1)(i)}$ is the effect range of fringing effects, and P_T is the spreading power from mode i to mode $(i-1)$ with the fixed $w_{S(i-1)}$.

If we call $S_{i\to i-1}$ and $S_{i\to i+1}$ are effect areas caused by mode i to mode $(i-1)$ and $(i+1)$, then

$$S_{i\to i-1} = \int_0^{l_{i-1}} \Delta S_i . dl \quad (9a)$$

$$S_{i\to i+1} = \int_0^{l_{i+1}} \Delta S_i . dl \quad (9b)$$

In case of n resonant modes antenna, there are only mode $i = 1$ and $i = n$ will affect the other adjacent modes similar as the above analysis, the remaining resonant modes $(i = 2, 3, \dots, n-1)$ in each component will be affected by the fringing effects of two modes put close to it as the model shown in Fig. 5, where x is the invasive distance caused by the fringing effects; l_i and w_{i_1} are length and interference area in the component i, respectively.

The area which affects to the component of mode i is determined as follows:

$$S_i = S_{i\to i-1} + S_{i\to i+1} - \bigcup (S_{i\to i-1}, S_{i\to i+1}) + l_i . w_{i_1} \quad (10)$$

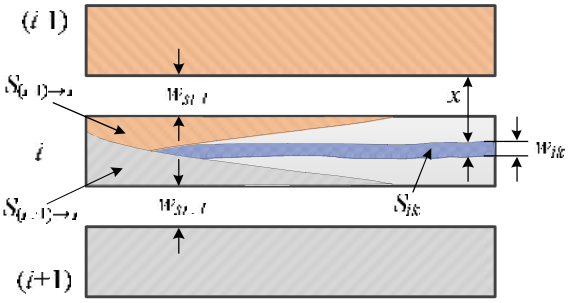

Fig. 5. Describing the fringing effects caused by mode $(i-1)$ and $(i+1)$ to mode i.

Now let consider the fringing effects in Fig. 5, the source of fringing effects includes power a_1 transmitted from mode $(i-1)$ to mode i and power a_2 transmitted from mode $(i+1)$ to mode i. The two aforementioned powers are different in magnitude and phase. The power of transmission wave in the area of width w_{i_1} is

$$a_\Sigma = a_1 + a_2 . e^{-j1\ \ c} = a_1 - a_2 \quad (11)$$

Thus, the invasive area in the component i can be determined as follows

$$S_\Sigma = S_{i\to i-1} + S_{i\to i+1} + S_{i_1} \quad (12)$$

where $S_{i_1} = l_i . w_{i_1}$

2.2. Proposed multiband antenna

The proposed antenna is a microstrip antenna which has two spiral strip branches shown in Fig. 6. The antenna is printed on FR4 substrate with a dielectric constant of 4.4 and thickness of 1.6 mm. Two spiral branches of the antenna are placed symmetrically in such a way that each spiral branch includes many segments different in width strip. The gap between the inner and outer segments are also different. These components will determine the resonant ability of segments when fringing effects occur. The octagonal metallic ground plane are cut perpendicular to the edge by two kinds of slot in which have the same widths and length of 3 and 11 mm, respectively.

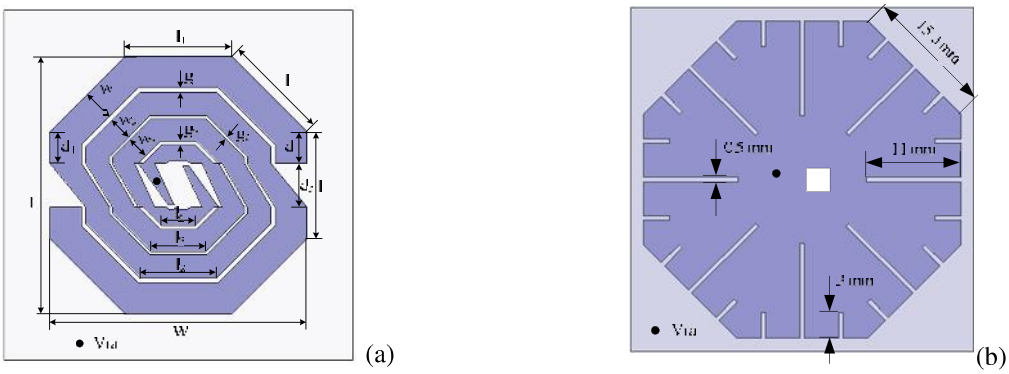

(a) (b)

Fig. 6. Model of proposed tri-band antenna.

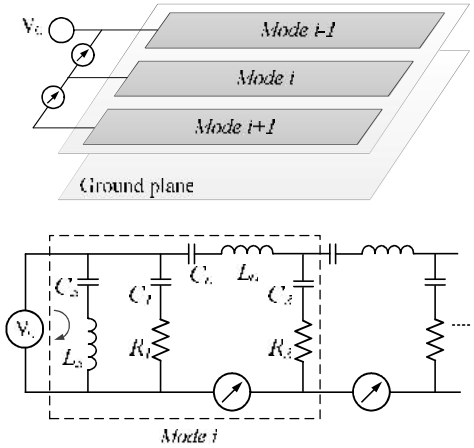

Fig. 7. Equivalent model and circuit of the proposed antenna corresponding resonant mode i.

The equivalent circuit of the proposed antenna is shown in Fig. 7. In particular, the capacitance C_3 is generated by the spiral strips and the metallic ground plane while inductance L_3 is formed by the metallic ground plane. The inductance L_0 is created by the segment corresponding to mode i. The capacitance C_1 và C_2 are made by the gap between the strip segments of mode i and mode $i-1$ and the gap between the strip segments of mode i and mode $i+1$, respectively. Equivalent impedance of mode i is defined as follows:

$$Z_i = \left(\frac{1}{\frac{1}{j\omega L_3} + j\omega C_3} + \frac{1}{R_1 + \frac{1}{j\omega C_1}} + \frac{1}{R_2 + \frac{1}{j\omega C_2} + j\omega L_0 + \frac{1}{j\omega C_0}} \right)^{-1} \tag{13}$$

Then we have,

$$\omega_i = \left[\left(R_1 R_2 + \frac{L_3}{C_2} + \frac{L_0}{C_3} + \frac{L_3}{C_0} + \frac{L_3}{C_1} \right) (R_2 L_3 + R_1 L_3 + R_1 L_0) \left(\frac{R_2}{C_3} + \frac{R_1}{C_3} + \frac{R_1}{C_2} + \frac{R_3}{C_1} + \frac{R_1}{C_0} \right) \left(\frac{1}{C_2 C_3} + \frac{1}{C_0 C_3} + \frac{1}{C_1 C_3} + \frac{1}{C_1 C_2} + \frac{1}{C_0 C_1} \right) L_0 L_3 \right]^{-\frac{1}{2}} \tag{14}$$

Thus, the resonant frequency of mode i is calculated by following equation,

$$f_i = \frac{\omega_i}{2\pi} \tag{15}$$

where ω_i is defined in Eq. (14).

2.3. Mutual induction and harmonic suppression

Model of mutual induction between two strips corresponding two different resonant modes is described in Fig. 8. The current flows in the strips is equivalent to inductance L, while the gap between two adjacent strips forms the coupling capacitance C. Moreover, capacitance C_f is created by the strips on the top and the ground plane on the bottom layer.

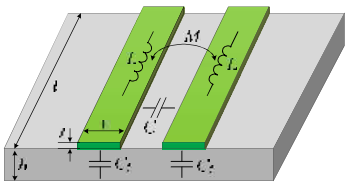

Fig. 8. Mutual induction model of two strip lines.

Thus, the resonant frequency of mode i is calculated by following equation The values of

capacitance C and C_f are determined by following equations:

$$C = \varepsilon_0.\varepsilon_r\left[0.03\left(\frac{W}{h}\right)+0.83\left(\frac{t}{h}\right)-0.07\left(\frac{t}{h}\right)^{0.2}\right]\left(\frac{S}{h}\right)^{-1.3} \quad (16)$$

$$C_f = \frac{\varepsilon_0.\varepsilon_r}{4}.M.\sqrt{1-\left(1+\frac{2W}{S}\right)^{-2}} \quad (17)$$

where, M is the coupling coefficient of two strips and can be calculated as follows,

$$M = \exp\left[\log(l)-\frac{1}{12}\left(\frac{W}{l}\right)^2+\frac{1}{60}\left(\frac{W}{l}\right)^4+\frac{1}{168}\left(\frac{W}{l}\right)^6\right] \quad (17a)$$

By applying the 1st Kirchhoff's law, we have:

$$\frac{\delta}{\delta}+\omega_0{}^2\int V.dt+\frac{V.\omega_0}{Q}\left[1-\frac{R_d.|V|}{R_1}\right]=\frac{\omega_0}{Q}.V_{ti} \quad (18)$$

where Q is quality factor of the circuit.

$$V = A(t).e^{j(\omega_0 t+\theta)} = A(t).e^{j\ (t)} \quad (18a)$$

$$\frac{\delta}{\delta} = V.\left[\frac{\mu.\omega_0}{2Q}(\alpha_0{}^2-|V|^2)+j\omega_0\right]+\frac{\omega_0}{2Q}.V_{ti} \quad (18b)$$

By inserting Eq. (18a) into Eq. (18b) we have,

$$\frac{\delta}{\delta} = \frac{\mu.\omega_0}{2Q}.A.(\alpha_0{}^2-A^2)+\frac{\omega_0}{2Q}.A.R_e\left(\frac{V_{ti}}{V}\right) \quad (19)$$

$$\frac{\delta}{\delta} = \omega_0+\frac{\omega_0}{2Q}.I_m\left(\frac{V_{ti}}{V}\right) \quad (20)$$

where,

$$V_{ti} = A_{ti}.e^{j(\omega_i\ t+\theta_i)} = A_{ti}.e^{j\theta_i} \quad (20a)$$

$$\omega_{ti}-\omega_0 = \Delta\omega.\sin\Delta t \quad (20b)$$

where,

$$\Delta\omega = \frac{\omega_0}{2Q}.\frac{A_{ti}}{A} \quad (20c)$$

is the differential frequency passing through the circuit with the frequency of the input signal.

Phase deviation of the signal is defined as

$$\Delta\theta = \pm\sin^{-1}\left(\frac{1}{2}\tan\theta\right) \quad (20)$$

3. Results and discussions

Firstly, this section presents simulated results and investigates the effect of antenna dimension to its resonant frequencies. The simulated results of return loss of proposed antenna is presented in Fig. 9. As can be seen, the proposed antenna has three resonant frequency bands with the -10dB bandwidth of (1.61 – 1.89) GHz, (2.29 – 2.64) GHz and (3.34 – 3.73) GHz. These frequency bands cover entirely the systems of 4G/1.8 GHz, WLAN/2.4 GHz and WiMAX/3.5 GHz.

To further analyze the role of the resonant elements in the proposed antenna, the simulation of electric field and current distribution of the antenna at the center resonant frequencies are done and presented in Fig. 10. As can be observed in this figure, the influence of fringing effects and mutual induction make the proposed antenna resonate at the various strip segments. The resonant areas are concentrated on the gap between the segments and the edge of segments of the antenna. By varying the gap, we can tune the resonant frequency ranges based on the density of the current or electric field distributed on the proposed antenna.

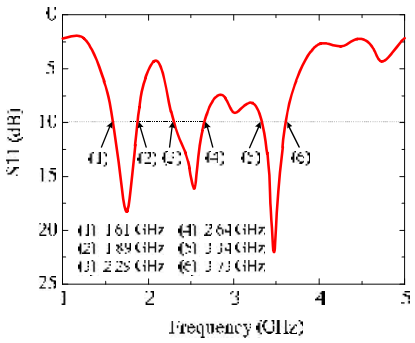

Fig. 9. Simulated S11 of proposed multiband antenna.

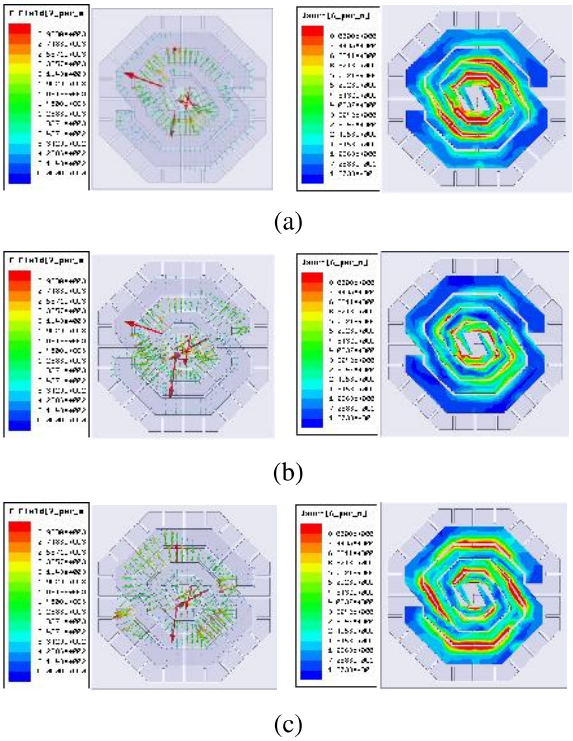

(a) (b) (c)

Fig. 10. Electric field (left side) and current distribution (right side) simulated of proposed at the center frequency of (a) 1.78 GHz, (b) 2.52 GHz, and (c) 3.58 GHz.

In order to consider the effect of dimension parameters on the reflection coefficient, different values are allocated to it. Note that, when one of these parameter changes other parameters are fixed. Fig. 11 plots the simulated magnitude of S11 of the proposed antenna versus the gap between the segments g_1, g_2 and g_3. It can be observed in Fig. 11(a), when the gap g_1 changes, the low frequency band (4G) almost unchanged, while the middle (WLAN) and high (WiMAX) frequency band were changed. This is consistent with the simulated results of electric field and current distribution shown in Fig. 10(a). Accordingly, the current (or electric field) distribution barely focuses on the gap g_1 at the low frequency band, but mainly focused on the middle and the high frequency band as the simulated results shown in Fig. 10(b) and (c).

In Fig. 11(b), the high frequency band is not significantly altered, however, the low and the middle frequency band are shifted as we change the value of g_2. This is entirely agreement with the simulation in Fig. 10, while in the gap g_2 current distribution is barely concentrated in the high frequency (Fig. 10(c)) but focusing on the middle and the low frequency band as the simulated results presented in Fig. 10(a) and (b). In case of S11 simulated results shown in Fig. 11(c), all three bands are shifted when changing the value of g_3. This can be explained by the simulated results in Fig. 10, in which the current density focus mostly on the gap g_3 at all three frequency bands. So, the change of the gap lead to the change of resonant frequency band and the S11 simulated results fully consistent with the current distribution examined at all three frequency bands.

The optimized parameters of proposed multiband antenna based on fringing effects of metamaterials are summarized in Table 1.

Radiation pattern simulated of the tri-band antennas is presented in Fig. 12. It is straightforward to recognize that the proposed antennas have an isotropic radiation pattern in H plane (YZ plane) with the simulated gain at 1.78, 2.45 and 3.58 GHz are 0.85, 2.36 and 3.92 dB, respectively.

Finally, the fabrication of the proposed antenna is presented in Fig. 13. The simulated and measured result of S11 of the proposed antenna are shown in Fig. 14. From this figure, it is observed that the antenna can operate at the -10 dB bandwidths of (1.70 – 1.96) GHz, (2.34 – 2.57) GHz and (3.43 – 3.78) GHz. The measured result of proposed antenna has a small deviation compared with simulation result due to the soldered SMA and fabrication technology. The total size of optimized antenna is 40 mm × 40 mm that is slightly larger than the tri-band antennas have proposed previously [11, 12], however, the proposed antenna is designed based on the novel methodology design and its size is compact enough for the applications of the advanced wireless communication systems.

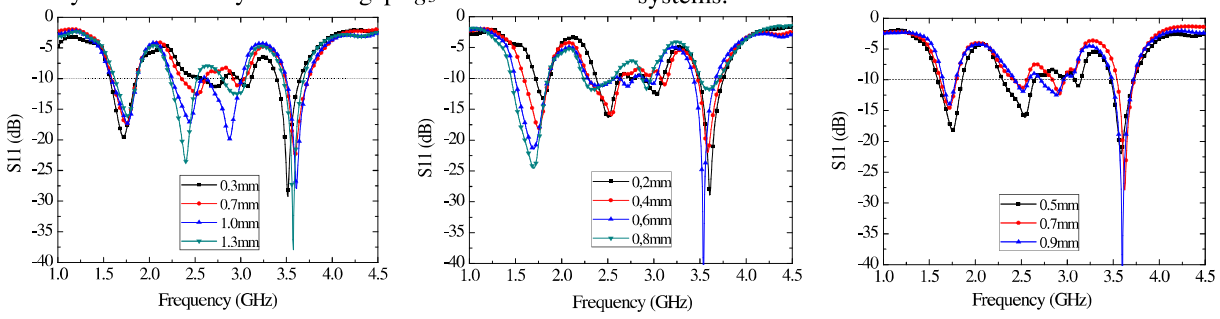

Fig. 11. Simulated S11 of proposed antenna versus different: (a) g1, (b) g2, and (c) g3.

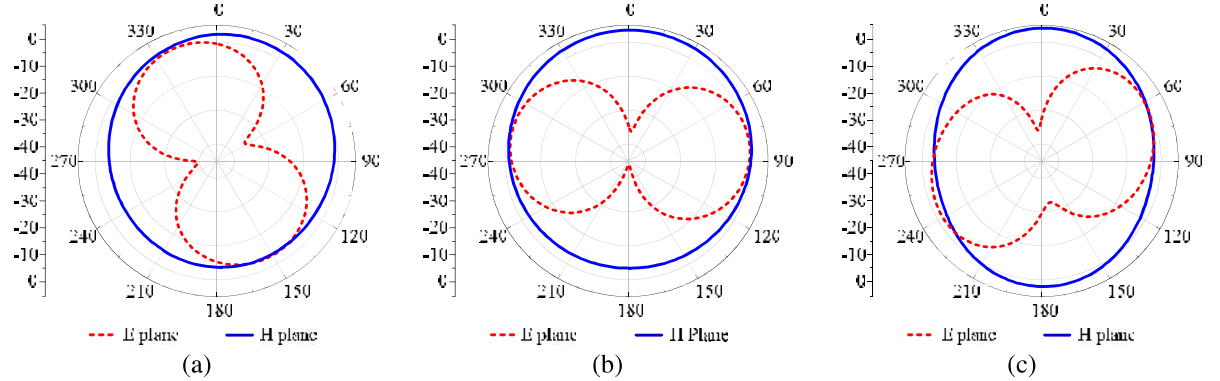

Fig. 12. Radiation pattern simulated of proposed antennas at frequency of (a) 1.78 GHz, (b) 2.45 GHz, and (c) 3.58 GHz.

Table 1. Optimized parameters of proposed tri-band antenna (Unit: mm).

W	29.56	w_1	3.6
L	29.56	w_2	2.68
l_1	12.24	w_3	2.5
l_2	8.8	g_1	0.55
l_3	6.28	g_2	0.37
l_4	3.82	g_3	0.46
d_1	3.62	d_2	5

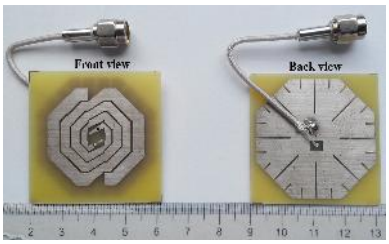

Fig. 13. Fabricated antenna.

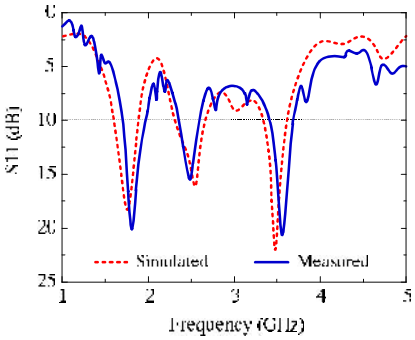

Fig. 14. Measured S11 of fabricated antenna.

5. Conclusion

This paper has proposed and shown the design of a novel multiband antenna using fringing effects of metamaterials. The proposed multiband antenna is a microstrip antenna with two spiral branches in which each spiral branch is constructed by many strip segments. The gaps between the segments of two branches are set at different values to create the resonances thanks to the fringing effects. Principle of mutual induction has been combined with fringing effects to analyze, calculate the resonant mode of the proposed antenna. Multi-band resonance is generated using mutual induction to suppress the harmonics. The measured S11 of fabricated antenna has been done. The result shows that the antenna resonates at three frequency bands of (1.70 – 1.96) GHz, (2.34 – 2.57) GHz and (3.43 – 3.78) GHz that are suitable with the systems of 4G/1.8 GHz, WLAN/2.4 GHz and WiMAX/3.5 GHz.

References

[1]. A. A. Eldek, "Analysis and design of a compact multi-band antenna for wireless communications applications," Microwave Journal, vol. 51, 2008.

[2]. C. Ghosh, S. Mondal, and S. Parui, "A compact multiband microstrip antenna using complementary slots on the ground plane," Microwave and Optical Technology Letters, vol. 58, pp. 47-51, 2016.

[3]. P. Mythili, P. Cherian, S. Mridula, and B. Paul, "Design of a Compact Multiband Microstrip Antenna," in 2009 Annual IEEE India Conference, 2009, pp. 1-4.

[4]. J.-W. Kim, T.-H. Jung, H.-K. Ryu, J.-M. Woo, C.-S. Eun, and D.-K. Lee, "Compact multiband microstrip antenna using inverted-L-and T-shaped parasitic elements," IEEE antennas and wireless propagation letters, vol. 12, pp. 1299-1302, 2013.

[5]. S. Asif, A. Iftikhar, M. N. Rafiq, B. D. Braaten, M. S. Khan, D. E. Anagnostou, and T. S. Teeslink, "A compact multiband microstrip patch antenna with U-shaped parasitic elements," in 2015 IEEE International Symposium on Antennas and Propagation & USNC/URSI National Radio Science Meeting, 2015, pp. 617-618.

[6]. K. Kumar and N. Gunasekaran, "A Compact Multiband Notch UWB Antenna," International Journal of Antennas and Propagation, vol. 2012, 2012.

[7]. K. Kiran, R. Yadahalli, R. Vani, S. F. Farida, and P. Hunagund, "Compact L-shaped notched printed antennas with dual slits for multiband and wideband applications," Microwave and Optical Technology Letters, vol. 49, pp. 2022-2026, 2007.

[8]. T. Hongnara, and M. Krairiksh, "A multiband CPW-fed slot antenna with fractal stub and parasitic line," Radioengineering, vol. 21, pp. 597-605, 2012.

[9]. Y. Kumar and S. Singh, "A Compact Multiband Hybrid Fractal Antenna for Multistandard Mobile Wireless Applications," Wireless Personal Communications, vol. 84, pp. 57-67, 2015.

[10]. P. S. R. Chowdary, A. M. Prasad, P. M. Rao, and J. Anguera, "Design and performance study of sierpinski fractal based patch antennas for multiband and miniaturization characteristics," Wireless Personal Communications, vol. 83, pp. 1713-1730, 2015.

[11]. Ya Wei Shi, Ling Xiong, and Meng Gang Chen, "Compact Triple-Band Monopole Antenna for WLAN/WiMAX-Band USB Dongle Applications," ETRI Journal, vol. 37, no. 1, Feb. 2015, pp. 21-25.

[12]. R. Wen, "Compact planar triple-band monopole antennas based on a single-loop resonator," in Electronics Letters, vol. 49, no. 15, pp. 916-918, July 18 2013.